第 30 卷 第 9 期 焊 接 学 报 Vol. 30 No. 9
2009 年 9 月 TRANSACTIONS OF THE CHINA WELDING INSTITUTION September 2009

纯铜与不锈钢扩散焊接头性能及原子扩散动态解析

刘树英
(河南科技大学 河南省有色金属材料科学与加工技术重点实验室, 河南 洛阳 471003)

摘 要: 采用微观组织观察、硬度测试、拉伸试验、EPMA(电子探针)等手段研究了焊接工艺条件对纯铜与铁素体 410L 以及奥氏体 304 不锈钢扩散焊接接头性能的影响, 结合理论计算对两种接头的原子扩散机理进行了解析. 结果表明, 在焊接压力、时间一定的条件下, 接头的抗拉强度随焊接温度的升高而增大. Cu 原子与 410L 最适宜的焊接温度比 Cu 原子与 304 的大约小 50 K, 这是由于 Cu 原子向体心立方晶体(bcc)铁素体系中的扩散速度比在面心立方晶体(fcc)奥氏体系中快的缘故. Cu 原子向不锈钢一侧扩散的实测值比理论值小是由于理论的初期条件是假定试样 100%完全密接, 而实际的接合界面却是粗糙不平, 要达到接合初期的完全密接是需要时间的.

关键词: 扩散焊接; 扩散速度; 铁素体; 奥氏体; 抗拉强度
中图分类号: TG456 文献标识码: A 文章编号: 0253—360X(2009)09—0101—04

刘树英

0 序 言

耐磨损性与强度兼备的计算机硬盘驱动器的轴动器, 由耐磨损性良好的铜合金与高强度的不锈钢经精密焊接制作完成. 这种动压轴动器与玉制轴相比可以减少共振点。随着这种新产品技术的开发, 可以预测不久的将来铜—不锈钢轴动器将会取代玉制轴动器. 耐磨损性与强度特性兼备, 高精度复合材料部件的研制, 首先被考虑和尝试使用的方法是扩散连接. 关于异种金属材料的扩散连接, 目前日本的研究虽然比较先进, 但纯铜与不锈钢扩散连接的研究也仅有少数需要精密接合的例子而已. 迄今为止, 关于纯铜与奥氏体不锈钢扩散连接的研究比较多, 一部分已被付诸于实用. 与此相对, 关于纯铜与铁素体不锈钢扩散连接的文献却极少, 而且这两者之间焊接性的差异和焊接机理并没有明确的被揭示[1—5].

文中考察、测试、分析了各种工艺参数对纯铜与两类不锈钢扩散焊接接头性能和微观组织的影响, 并结合理论计算, 对焊接工艺参数与接头强度以及接合界面及附近原子扩散行为的关联性进行了揭示、比较、探讨, 阐明了纯铜与铁素体及奥氏体不锈钢两者之间焊接性存有差异的原因及焊接机理, 以便为耐磨损性(或者是热传导性)与强度兼备的复合材料部件的研制提供理论与技术参考.

1 试验方法

试验使用的材料是纯铜(无酸素铜)和低碳铁素体系不锈钢 410L、奥氏体系不锈钢 304, 这些材料的化学成分见表 1.

表 1 纯铜和不锈钢的化学成分(质量分数, %)
Table 1 Chemical composition of pure Cu and stainless steel

	Cu	C	Si	Mn	P	S	Ni	Cr	Fe
纯铜	>99.99	—	—	—	—	—	—	—	—
410L	—	0.015	0.59	0.87	0.015	0.001	0.2	12.56	余量
304	—	0.05	0.46	1.00	0.03	0.09	8.39	18.09	余量

将试验材料加工成 10 mm×20 mm×20 mm 的试样, 接合面用纱纸将其湿式研磨后, 进行了精磨和抛光. 确认接合面没有擦痕成为镜面后即可作为焊接试样. 焊接前在丙酮中进行超声波清洗、脱脂后, 放置于真空扩散接合装置中, 待达到 6.7×10^{-3} Pa 的真空度后实施扩散焊接. 主要的扩散焊接工艺参数见表 2.

收稿日期: 2008—10—15

表 2 主要扩散焊接条件

Table 2 Main diffusion bonding conditions

试样	焊接温度 T/K	焊接压力 p/MPa	焊接时间 t/ks
Cu/410L	1 073, 1 123, 1 173, 1 223	4.9	3.6
Cu/410L	1 223	4.9	7.2
Cu/410L	1 073, 1 123	7.8	3.6
Cu/410L	1 023	9.8	3.6
Cu/304	1 123, 1 173, 1 223, 1 273	4.9	3.6

为了评价接头的性能,进行了常温拉伸试验,以接合界面为主的光学显微镜微观组织观察、显微硬度测定.为了调查原子的扩散进展状况,进行了接合界面附近的 EPMA 面分析以及线分析.为了探讨铁以及铜的扩散现象,应用 Fick 的第 2 法则对扩散距离(x)和浓度(C)的关系由下式作了计算[6,7],即

$$C/C_s = \mathrm{erfc}(x/2\sqrt{Dt})$$

式中:C_s 为初期浓度;D 为扩散系数;t 为扩散时间,初期条件 $t=0$ 时,$x<0$, $C=1$, $x>0$, $C=0$.

2 试验结果与分析

2.1 纯铜与铁素体不锈钢 410L 的扩散焊接

图1是焊接温度与接头抗拉强度的关系.在焊接压力 4.9 MPa、焊接时间 3.6 ks 一定的条件下,随着焊接温度的升高,抗拉强度增加,在 1 173 K 取得最大值,而在 1 223 K 又稍有下降.断裂位置到 1 123 K 为止是在焊接界面,而在 1 173 K 以上却是纯铜母材部位.即在试验的工艺参数内,最适宜的焊接温度是 1 173 K.这主要是由于随温度的升高,焊接界面附近原子进一步的充分扩散,扩散距离也增大,并且由相互扩散形成的合金层厚度也逐渐增加的缘故.而另一方面,在焊接温度 1 223 K,抗拉强度稍有下降可以认为是因为母材是纯铜,随焊接温度的上升而发生软化致使其抗拉强度有所下降所致.

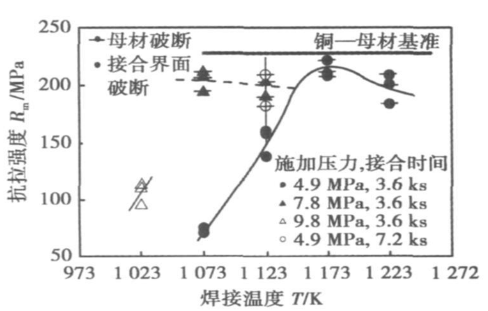

图 1 Cu/410L 焊接条件与抗拉强度的关系

Fig. 1 Relationship between bonding conditions and tensile strength of Cu/410L joints.

由图 1 还可以看出,当焊接压力加大到 7.8 MPa、焊接时间仍为 3.6 ks 时,焊接温度为 1 073 K,抗拉强度变大,获得母材破断的强度.此豌由图还可知,在焊接压力 4.9 MPa、焊接温度 1 123 K 的情形下,将焊接时间延长到 7.2 ks 时,抗拉强度也增大,同样也获得母材破断的强度.但是,若将焊接压力进一步加大到 9.8 MPa、焊接时间仍为 3.6 ks,而将焊接温度降低至 1 023 K 时,却从接合界面开裂破断了,即将焊接压力加大,或将焊接时间延长,虽然均可使母材破断的焊接温度降低,但基本存在一个最低温度极限.总之在此项研究范围内母材破断的最低焊接温度是 1 023 K 以上.

图 2 是焊接压力 4.9 MPa、焊接时间 3.6 ks 的接合界面附近的微观组织.由图可见,在焊接温度为 1 073 K, 1 123 K 的条件下,接合界面间微小的间隙可以被观察到,表明接合是不充分的.另一方面,在焊接温度为 1 173 K 和 1 223 K 的条件下,接合界面的密接化进一步提高,特别是在 1 173 K 时,接合缺陷观察不到,界面密切接触几乎融为一体,焊接性良好的事实是清晰的.

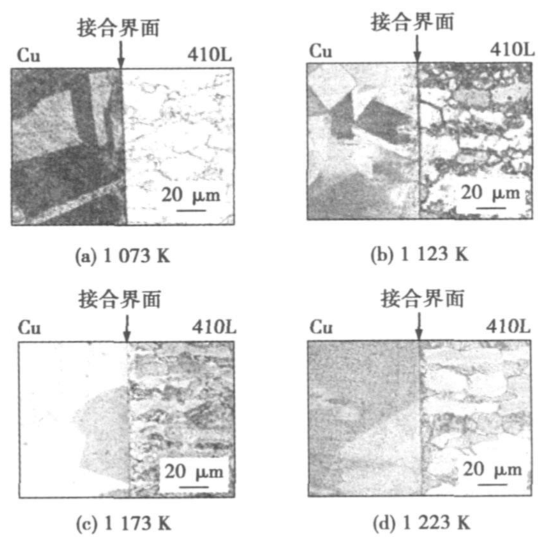

图 2 Cu/410L 接合界面及附近的微观组织

Fig 2 Microstructure near bonding interface of Cu/410L joints.

图 3 是焊接压力为 4.9 MPa、焊接时间为 3.6 ks、焊接温度为 1 073 和 1 173 K 下的微型维氏硬度测定结果.由图 4 可知,接合界面附近的硬度与母材的硬度几乎没有区别,所以推定在接合界面间没有金属间化合物的形成[8].

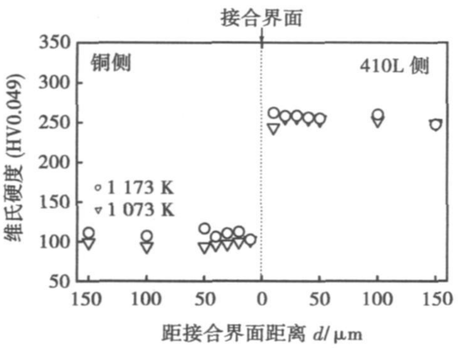

图 3　Cu/410L 接合界面的距离与硬度的关系

Fig. 3　Relationship between distance from bonding interface and Vickers hardness of Cu/410L

图 4 是焊接压力为 4.9 MPa、焊接时间为 3.6 ks、焊接温度为 1 073 和 1 173 K 条件下, EPMA 面分析浓度分布测定结果. 由图可知, Fe 和 Cu 原子都有不同程度的扩散, 其扩散进展状况与扩散温度等有关.

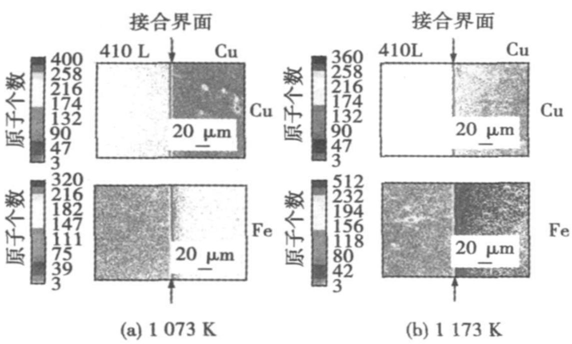

图 4　Cu/410L 接头的 EPMA 分析结果

Fig. 4　Results of EPMA for Cu/410L joints

图 5 是关于 Fe, Cu 原子浓度分布的 EPMA 线分析实测值与根据 Fick 的第 2 法则求得的理论值的比较结果. 图中, 粗线的实、点线分别代表 1 173 K 铜向不锈钢一侧扩散的理论值与实测值. 细线的实、破点线分别代表 1 073 K 的理论值与实测值. 由图可知, 向不锈钢一侧扩散的铜的实测值比理论值要小; 同样, 向铜一侧扩散的铁的实测值也比理论值要小. 即无论在任何温度下实测值均比理论值要小, 而且, 越是高温其实测值与理论值的差越大. 实测值比理论值小的原因是由于理论的初期条件是假定两试样最初是 100%密切接触的. 而实际的两接触界面却是凹凸(表面粗糙)不平, 要达到 100%的密接是需要时间的.

实际的扩散比理论上要慢. 而且, 越是高温其实测值与理论值的差越大的原因是由于理论值是以铁素体系的扩散来计算的, 而实际上越是接近高温, 由铁素体系向奥氏体系转变的可能性是存在的, 受之影响越是高温其实测值与理论值差值增大的倾向也越大[9].

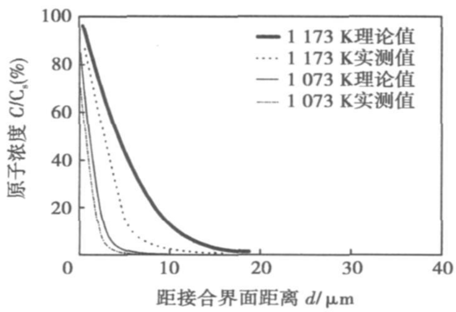

图 5　Cu/410L 接头不锈钢侧铜的浓度分布

Fig 5　Concentration distribution of Cu at stainless steel side of Cu/410L joints.

2.2　纯铜与奥氏体不锈钢 304 的扩散焊接

图 6 是焊接温度与接头抗拉强度的关系以及各焊接温度下接合界面附近的显微组织观察结果. 在焊接压力为 4.9 MPa、焊接时间为 3.6 ks 的条件下, 随着焊接温度的升高抗拉强度也增大, 在 1 223 K 时取得最大值, 而在 1 273 K 又稍有下降. 这正如从微观组织观察中看到的从 1 123 ~ 1 223 K, 接合界面的密接化程度进一步提高, 特别是与 1 223 K 时密接良好的事实对应. 断裂位置到 1 173 K, 60%是在接合面, 40%在纯铜母材部位, 而在 1 223 K 以上却完全是在纯铜母材部位. 即在这种场合下, 最适宜的焊接温度是 1 223 K.

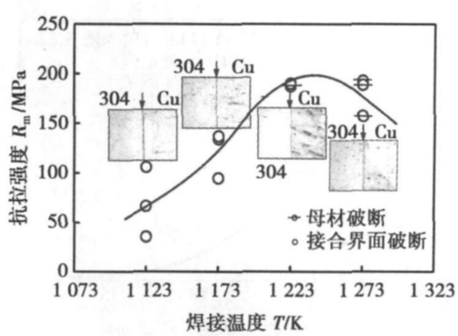

图 6　Cu/304 焊接温度与抗拉强度的关系

Fig 6　Relationship between bonding temperature and tensile strength of Cu/304 joints.

3 Cu/410L 与 Cu/304 扩散焊接头强度特性的比较和探讨

3.1 接头强度特性的比较和探讨

图7 为铁素体系 Cu/410L 与奥氏体系 Cu/304 除焊接温度外其它工艺参数一定的抗拉强度的对比结果. 由图可见, 抗拉强度的最大值对应的最适宜的焊接温度对于 410L 而言是 1 173 K, 而对于 304 而言基本是 1 223 K. 即最适宜的焊接温度铁素体系 410L 比奥氏体系 304 大约小 50 K。而且 Cu/410L 组合抗拉强度的最大值比 Cu/304 大约大 25 MPa.

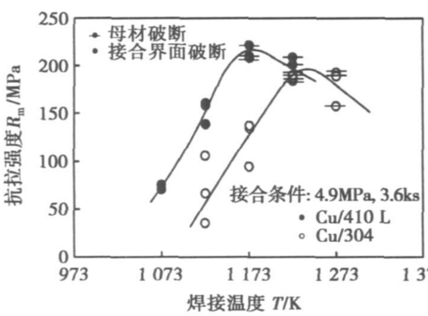

图 7 Cu/410L 与 Cu/304 焊接温度与抗拉强度的关系

Fig. 7 Relationship between bonding temperature and tensile strength of Cu/410L and Cu/304.

Cu/410L 的最大抗拉强度比 Cu/304 大的原因如前所示, 是由于该组合最合适的焊接温度比较低、铜母材的抗拉强度大的缘故, 即也可以认为是母材的软化比较小的缘故.

3.2 Cu 原子向不锈钢中的扩散速度分析

图8 是焊接工艺一定的条件下, Cu/410L 与 Cu/304 不锈钢一侧纯铜的浓度分布对比结果. 如图所示, 纯铜向不锈钢一侧的扩散速度表现为理论值以及实测值均为 410L 比 304 大. 原因是由于 Cu 原子向 410L 一侧的扩散其 410L 是体心立方晶体结构(bcc), 振动频率(系数)据记载为 4.2×10^{-4}; 而 Cu 原子向 304 一侧的扩散却由于 304 是面心立方晶体结构(fcc), 振动频率(系数)据记载为 4.3×10^{-5}[9]. 由此可知, 向不锈钢一侧扩散的 Cu 原子的扩散速度, 在 bcc 的铁素体系中比在 fcc 的奥氏体系中要快.

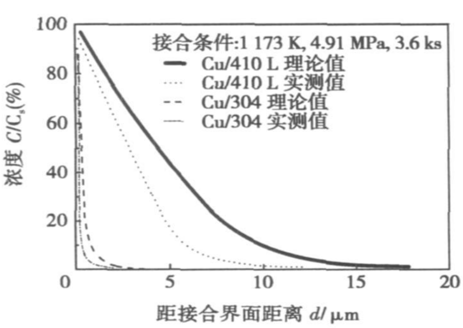

图 8 Cu/410L 与 Cu/304 接头不锈钢侧铜的浓度分布

Fig. 8 Concentration distribution of Cu at stainless steel side for Cu/410L and Cu/304.

4 结 论

(1) 纯铜与 410L 的扩散焊接, 接头的抗拉强度在焊接压力、焊接时间一定的情况下, 随焊接温度的升高而增大, 但适度的温度以上又会下降. 将焊接压力增大或将焊接时间延长, 可以在较低的焊接温度下获得纯铜母材部位断裂的良好的扩散焊接接头.

(2) Cu 原子向不锈钢一侧的扩散, 或不锈钢中的 Fe 原子向纯铜一侧扩散的实测值比由 Fick 的第 2 法则求得的理论值要小. 这是由于理论计算的初期条件是假定两试样最初是 100%密切接触。而实际的接触界面却是粗糙不平, 可以推测要达到初期假设的完全密接是需要时间的.

(3) 除焊接温度以外的其它焊接工艺参数一定的条件下, Cu/410L 扩散连接的最适宜的焊接温度比 Cu/304 的大约小 50 K.

参考文献:

[1] Nishimoto Kazutoshi, Natsume Matsuware. Welding of stainless steel[M]. Tokyo: Sanbou Publish, 2001.

[2] Kazutoshi O. Welding actually of stainless steel[M]. Tokyo: Sanbou Publish, 1995.

[3] Seto Satuo. Diffusion bonding between Cu and stainless steel[J]. Ishikawa Jima-Harima Wazahou. 1984, 22(3): 1-6.

[4] Oohasi Osa. Diffusion bonding between Cu and tungsten[J]. Welding Society Thesis Collection, 1998, 16(3): 319-323.

[5] Qin Caidong, Brian Derby. Diffusion bonds between a stainless steel and zirconia[J]. Journal of Americal Ceramic Society, 1993, 76(11): 232-234.

[6] Saito Muokayuki. Formation of tissue and diffusion equation[M]. Tokyo: Sanbou Publish, 1985.

[7] Paul G. Shewmon original works: diffusion within solid[M]. Toky: 海文堂出版, 2005.

[8] Japanese Material Science Society. Intermetallic compound and material[M]. Tokyo: 裳华房出版, 1995.

[9] Japanese Metallic society. Metallic data book. the third revision edition[M]. Tokyo: Maruzen, 1993.

作者简介: 刘树英, 女, 1961 年出生, 博士, 副教授. 主要从事异种材料的焊接和金属热处理. 发表论文 10 篇.

Email: Liusy168@yahoo.com.cn

determined. Effect of argon arc remelting parameters on microstructure and mechanical properties of hot dipping aluminizing surface was investigated. The results show that, for the hot dipping aluminizing coating after argon arc remelting treatment, stratification phenomenon disappeared, gradient transition on microstructure appeared, specimen consisted of remelting layer, transition layer and substrate. Argon arc remelting treatment can obviously increase microhardness of hot dipping aluminizing coating. The process parameters influence the depth, hardness and crack rate of the remelting layer markedly. With the welding current increasing or the welding speed decreasing, the remelting layer depth and hardness increases, and the crack rate decreases.

Key words: hot dipping aluminizing (HDA); argon arc remelting; microstructure; microhardness

Simulation of viscoelastic heat during ultrasonic welding of thermoplastics ZHANG Zhenqiang[1], ZHANG Zongbo[1], LUO Yi[1,2], WANG Xiaodong[1,2], WANG Liding[1,2] (1. Key Laboratory for Precision and Non-traditional Machining Technology of Ministry of Education, Dalian University of Technology, Dalian 116024, Liaoning, China; 2. Key Laboratory for Micro/Nano Technology and System of Liaoning Province, Dalian 116024, Liaoning, China). p 97—100

Abstract: Viscoelastic heat is one of the main heat sources during ultrasonic welding of thermoplastics. Unfortunately the present works could not definitely take into account the dynamic viscoelasticity of thermoplastics. In this paper a simplified method was proposed to characterize dynamic viscoelasticity based on static relaxation modulus and TTEP (time-temperature equivalent principle). The method could represent dynamic modulus as the function of temperature and frequency, and avoids calculating dynamic modulus of high frequency by shifting and extrapolating the dynamic modulus of lower frequency from experiments. With the method mentioned above, a strategy was put forward to simulate the viscoelastic heat of PMMA (polymethyl methacrylate) under periodic load using FEM (finite element method). The calculated temperature shows a similar tendency as tested results in other literatures.

Key words: ultrasonic welding; dynamic viscoelasticity; viscoelastic heat; finite element method

Joints performance of diffusion bonding between pure Cu and stainless steel and dynamic analysis of atomic diffusion LIU Shuying (Key laboratory of Advanced Non-ferrous Metals, Henan University of Science and Technology, Luoyang 471003, Henan, China). p 101—104

Abstract: The effects of welding parametas on the performance of the joints of pure copper and ferrite 410L and joints of pure copper and austenite 304 stainless steel were researched by microstruture observation, hardness, tensile test and EPMA. And atomic diffusion mechanism of two kinds of joints combined theoretical calculation was also discussed. The result indicated: as bonding pressure and bonding time fixed, the joints tensile strength increased with the bonding temperature. Optimal bonding temperature of Cu/410L is about 50 K lower than that of Cu/304, because the diffusion speed of Cu, bcc ferrite is faster than in fcc austenitic. The measured diffusion speed of Cu atom in stainless steel is smaller than the theoretical value because the theoretical value was obtained based on assuming 100% full adhesion for the surface in initial, but the actual bonding surface is rough in initial stages.

Key words: diffusion bonding; diffusion speed; ferritic; austenitic; tensile strength

Microstructure and properties of 65Mn spring steel by laser welding LIU Qibin, LI Bin (Materials School of Guizhou University, Caijiaguan Branch, Guiyang 550003, China). p 105—108

Abstract: To obtain excellent welding joint, 65Mn spring steel was welded by 5 kW CO_2 laser welding equipment. Microstructure, tensile strength, tensile fracture and residual stress of this joint were investigated by means of OM, XRD, SEM, microhardness testing machine, electronic universal testing machine and residual stress test machine. The experimental results indicate that the fine equiaxised crystal, dendrite crystal and cell grain are formed from welding central zone to edge zone, respectively. In the HAZ, the over-heated zone is mainly comprised of coarse acicular martensite. Recrystalline zone mainly consistes of fine acicular martensite. The part transforming zone is comprised of ferrite and pearlite. The welding joint mainly consists of fine α-Fe, Fe_3C and FeSi. The highest hardness value of welding zone and HAZ is 720 HV and 770 HV, respectively. The hardness decreases significantly from HAZ to base metal. The average tensile strength of welding joints is approximately 475 MPa. The average residual stress in welding zone is 105 MPa, and the average residual stress in HAZ is −60 MPa.

Key words: spring steel; 65Mn; laser welding; microstructure; properties

Prediction for welding deformation reducing by welding sequence optimization of upper plate ZHOU Guangtao[1,2], LIU Xuesong[2], YAN Dejun[2], FANG Hongyuan[2] (1. College of mechanical Engineering and Automation, Huaqiao University, Xiamen 361021, China; 2. State Key Laboratory of Advanced Welding Production Technology, Harbin Institute of Technology, Harbin 150001, China). p 109—112

Abstract: The numerical simulation of welding deformation of upper plate structure for large-scale crane box beam was conducted using the thermo elastic-plastic method. Analysis model was established to quantitatively describe the effects of welding sequence for both longitudinal rib to upper plate and transverse rib to upper plate on welding deformation. The optimal welding sequence of the whole structure was obtained by the term of the "and" relation. The simulation value of deformation under the optimal welding sequence was contrast to measured value to show the better agreement for two values. The deformation of the optimal sequence and the worst sequence was 15.12 mm and 28.47 mm, respectively.

Key words: numerical simulation; welding sequence; optimal; prediction